CrossMark

Biodegradability of the anticancer drug etoposide and identification of the transformation products

Tina Kosjek[1,2] · Noelia Negreira[3] · Ester Heath[1,2] · Miren López de Alda[3] ·
Damià Barceló[3,4]

Abstract Etoposide susceptibility to microbiological breakdown was studied in a batch biotransformation system, in the presence or absence of artificial wastewater containing nutrients, salts and activated sludge at two concentration levels. The primary focus of the present study was to study etoposide transformation products by ultra-high performance liquid chromatography coupled to high-resolution hybrid quadrupole-Orbitrap tandem mass spectrometry (MS/MS). Data-dependent experiments combining full-scan MS data with product ion spectra were acquired to identify the molecular ions of etoposide transformation products, to propose the molecular formulae and to elucidate their chemical structures. Due to the complexity of the matrix, visual inspection of the chromatograms showed no clear differences between the controls and the treated samples. Therefore, the software package MZmine was used to facilitate the identification of the transformation products and speed up the data analysis. In total, we propose five transformation products; among them, four are described as etoposide transformation products for the first time. Even though the chemical structures of these new compounds cannot be confirmed due to the lack of standards, their molecular formulae can be used to target them in monitoring studies.

Keywords Etoposide · Biodegradation · Transformation product · Mass spectrometry · Orbitrap · Transformation · Wastewater

✉ Tina Kosjek
  tina.kosjek@ijs.si

1 Department of Environmental Sciences, Jožef Stefan Institute, Jamova 39, Ljubljana, Slovenia

2 Jožef Stefan International Postgraduate School, Jamova 39, Ljubljana, Slovenia

3 Water and Soil Quality Research Group, Department of Environmental Chemistry, Institute of Environmental Assessment and Water Research (IDAEA-CSIC), Jordi Girona 18-26, E-08034 Barcelona, Spain

4 Catalan Institute for Water Research (ICRA), H2O Building, Scientific and Technological Park of the University of Girona, Emili Grahit 101, 17003 Girona, Spain

Introduction

Cytostatic chemotherapy drugs, also referred to as anticancer or antineoplastic agents, are routinely used in chemotherapy and enter wastewater through the excretion of the non-metabolised drug following administration to patients. The fate of these compounds in the environment is largely unknown, but they can reach aquatic ecosystems via wastewater treatment effluents (Zounková et al. 2007). They are of particular environmental concern because of their potential carcinogenicity, mutagenicity and genotoxicity (Zounková et al. 2007; Kosjek and Heath 2011). They also enter the environment as mixtures of parent compounds, metabolites and transformation products (TPs), where studies have shown that TPs are in some cases more toxic and persistent (Donner et al. 2013).

Etoposide (ETP) is a semisynthetic epipodophyllotoxin derivative (Beijnen et al. 1988) considered to be one of the most effective agents against a diverse array of neoplastic diseases including small-cell lung cancer, testicular cancer and lymphomas (Akhtar et al. 2013). Its mechanism of action involves breakage of DNA strands by reversible interaction with

topoisomerase II (Hande 2008). Chemically ETP is designated as 4′-demethylepipodophyllotoxin-9-(4,6-O-ethylidene)-β-D-glucopyranoside. The major part of the molecule includes a tetracyclic ring system that consists of tetrahydronaphthalene (B+C), with attached γ-lactone ring (D) on one side and a dioxolane ring (A) on the other side. The tetrahydronaphthalene links 4′-hydroxy-3′,5′-dimethoxyphenyl (E) on position 3 and a glycoside ethylidene-glucopyranoside (G+F) on position 9 (Fig. 1).

After absorption in the human body, ETP undergoes a cytochrome P-450-dependent metabolism, which converts the compound into its O-demethylated metabolite (Haim et al. 1987). Urinary excretion of this metabolite has been reported to be minor: About 50 % of an intravenous dose of ETP is recovered in urine; up to 17 % is excreted as a glucuronide metabolite and less than 2 % as the 3′-O-desmethyl-etoposide metabolite (Holthuis et al. 1986).

Since ETP is used for cancer treatment of hospitalised patients, excretion of the mixture of parent compound and metabolites from the body takes place mainly at hospitals. Typically, discharges of effluents from hospitals reach the municipal sewerage system after simple disinfection, where elimination of cytostatic drugs is often incomplete and residues eventually enter surface waters (Franquet-Griell et al. 2015, Kosjek et al. 2013). A literature review reveals only a limited number of studies on the occurrence of ETP in wastewaters and receiving surface waters, where mostly hospital effluents are addressed. Yin et al. (2010) investigated 21 hospital effluents from Beijing, China and reported ETP levels from 6 to 380 ng/L. ETP was also reported in a hospital effluent in Girona (northeast of Spain) at levels up to 714 ng/L (Ferrando-Climent et al. 2014). In a wastewater treatment plant (WWTP), influent ETP levels were lower, up to 83 ng/L (Ferrando-Climent et al. 2013; Martin et al. 2011). Overall, data about the output levels of ETP from WWTPs are still scarce. ETP has only been reported in one effluent from a municipal WWTP plant in Seville (south of Spain), at a level of 3.4 ng/L (Martin et al. 2011), which implies that it may be degraded during wastewater treatment. To our knowledge, only two studies attempted to determine ETP in surface waters both reporting ETP levels <LOD (Martin et al. 2011; Ferrando-Climent et al. 2014). Reported data are in good agreement with predicted environmental concentrations (PEC) for ETP in effluents (0.53 ng/L) and rivers (0.02 ng/L) reported by Franquet-Griell et al. (2015).

The only study addressing ETP treatment (Negreira et al. 2015a) demonstrated that ETP reacts quickly with the free chlorine present in water leading to the formation of two oxidation TPs. One of them corresponded to the metabolite 3′-O-desmethyl-etoposide and was found in several river and wastewater samples at levels between 14 and 33 ng/L, whereas the parent compound ETP was not detected in any of the samples. The presence of this TP/metabolite in the aquatic system was attributed mainly to its formation in the presence of free chlorine (Negreira et al. 2015b), since its presence in urine was reported to be minimal (Holthuis et al. 1986). To our knowledge, there are no studies available in the literature addressing other ETP treatments including biodegradation.

The present study aims to contribute to the existing knowledge on fate of ETP, when exposed to microorganisms, and, in particular, to identify TPs formed during biodegradation. We studied the susceptibility of ETP to biodegradation under specific conditions, including the presence or absence of a carbon source and with varying amounts of activated sludge (AS). Our main focus was on the formation, detection, and identification of TPs during biotransformation experiments.

Experimental

Caution: ETP has been classified by the International Agency for Research on Cancer (IARC) in Group 1 as a substance carcinogen to humans (2012) and should be handled with care.

Standards and chemicals

ETP [4′-demethylepipodophyllotoxin-9-(4,6-O-ethylidene)-β-D-glucopyranoside; CAS 33419-42-0] was of ≥99 % purity, whereas deuterated ETP (ETP-d3) was 98 % pure and with the isotopic purity of 99 %. Both compounds were obtained from Santa Cruz Biotechnology (CA, USA). All solvents and chemicals used for chromatographic separation (methanol, water, formic acid) and chemicals used for biomass inhibition (formaldehyde (FDH)) or standard dissolution (dimethyl sulfoxide (DMSO)) and nutrient-mineral medium (yeast and meat extract, casein peptone, CH_3COONH_4, NH_4Cl, K_2HPO_4, KH_2PO_4, $CaCO_3$, $MgCO_3$, $NaCl$, $FeSO_4 \cdot 7H_2O$) were of analytical reagent grade purity. Individual
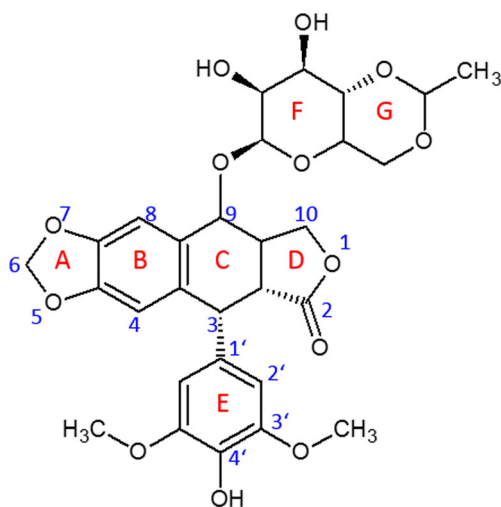

Fig. 1 Chemical structure of ETP

stock solutions (approx. 1000 mg/L) were prepared in DMSO and stored in amber glass vials at −20 °C. Different working standard solutions were freshly prepared on the day of the experiments by appropriate dilution in DMSO and ultrapure water.

Setup of the biotransformation experiments

Biodegradability of ETP was studied by conducting batch biotransformation experiments in 0.5-L glass bottles (total wetted volume of 0.4 L), which were aerated with an aquarium pump. The amount of dissolved oxygen was 7.4 ± 1.6 mg/L. The experiments were performed at room temperature and protected from light. AS used in the biotransformation experiments was obtained on the day of their setup from a nitrification basin at a WWTP treating 22–30 million m^3 of wastewater per year (360,000 population units). Wastewater from this WWTP originates mostly from municipalities, stormwater, hospitals and health centres, pharmaceutical and food industry and waste recycling. Upon arrival to our laboratory, the AS was allowed to settle, and 50 or 10-mL inoculums of the AS were added into the test bottles. FDH was added where applicable (Table 1), and the solution was left to shake for more than 4 h in order to allow the complete biomass inhibition (Süzer 2013). Deionised water (DIW) was added as the alternative to FDH to account for the identical total volume in each test bottle.

The experiments were performed in nutrient-mineral or salt-only medium, and to account for possible abiotic degradation and sorption, control experiments were run in DIW

with (E) or without (E2) the addition of FDH (Table 1). Four hundred microlitres of 1 mg/mL ETP solution in DMSO was added to the 0.4 L test solutions to give a final concentration of 1 mg/L ETP, whereas the concentration of DMSO did not exceed 0.1 % of the total volume of the test solution. The detailed description of the experimental setup is given in Table 1.

The nutrient-mineral medium mimicked the composition of a municipal wastewater and contained yeast and meat extract, casein peptone, ammonium acetate and salts NH_4Cl, K_2HPO_4, KH_2PO_4, $CaCO_3$, $MgCO_3$, $NaCl$ and $FeSO_4 \cdot 7H_2O$. The detailed description of the nutrient-mineral medium is given elsewhere (Kosjek et al. 2007). As evident from Table 1, the nutrient-mineral medium was applied in the tests A, B, A2, B2 and in both blanks, whereas minerals only, with no addition of the carbon source, were added into the test bottles C, D, C2 and D2. The pH was in the range of 6.3 (ETP-E2, deionised water) to 8.0 (ETP-A, nutrient-mineral medium).

AS concentration was determined at the end of the biotransformation tests by filtering 15 mL of each homogenised sample through glass microfibre filters (MN GF-3, Machery Nagel, Düren, Germany) that were previously dried at 105 °C to constant weight. After filtration, the filters with AS residue were again dried to constant weight, and the concentration of AS was calculated as the difference in weight prior to and post filtration.

Sampling was performed by withdrawal of 4 mL of samples from the reaction bottle at the setup of the experiments and on eight consecutive days at approximately 24-h intervals. Samples were immediately frozen and were stored in 10-mL PTFE vials until analysis.

Table 1 Design of the biodegradation experiments

Sample	AS inoculum (mL)	AS concentration (g/L)	Nutrient-mineral medium (mL)	Mineral medium (mL)	DIW (mL)	Addition of 40 % (v/v) FDH (mL)	Addition of ETP	Total V (mL)
ETP-A	50	2.6	290	0	60	0	1 mg/L	400
ETP-B	50	2.9	290	0	0	60	1 mg/L	400
ETP-C	50	1.8	0	290	60	0	1 mg/L	400
ETP-D	50	2.8	0	290	0	60	1 mg/L	400
ETP-E	0	0	0	0	340	60	1 mg/L	400
BLANK-50	50	1.9	290	0	60	0	No addition	400
ETP-A2	10	0.59	330	0	60	0	1 mg/L	400
ETP-B2	10	0.52	330	0	0	60	1 mg/L	400
ETP-C2	10	0.44	0	330	60	0	1 mg/L	400
ETP-D2	10	0.43	0	330	0	60	1 mg/L	400
ETP-E2	0	0	0	0	400	0	1 mg/L	400
BLANK-10	10	0.48	330	0	60	0	No addition	400

Sample preparation

Samples were filtered through 0.2-μm regenerated cellulose filters (Phenomenex), and 300 μL of the samples was transferred into the vials. After addition of the internal standard ETP-d3 at the final concentration of 0.2 μg/mL, the samples were injected into the LC-MS.

LC-MS analysis

The Waters Acquity ultra-high performance liquid chromatograph (UHPLC, Milford, MA, USA) coupled to the Thermo Scientific Q Exactive hybrid quadrupole-Orbitrap[TM] (San Jose, CA, USA) mass spectrometer was used for the separation and identification of the TPs. The chromatographic separation of the samples was performed on a reversed-phase UHPLC column Hibar HR (50 × 2.1 mm, 2 μm particle size) from Merck (Darmstadt, Germany). The mobile phases employed in electrospray-positive (ESI(+)) analysis were (A) water with 0.1 % formic acid and (B) methanol with 0.1 % formic acid, whereas the electrospray-negative (ESI(−)) analysis was accomplished with no addition of formic acid. Elution was performed with the following solvent gradient: 0–1 min, 5 % B; 3 min, 20 % B; 6, 80 % B; 7 min, 100 % B; 10–12 min, 5 % B. The flow rate was 300 μL/min, and the injection volume was 10 μL.

The ESI was operated in both polarity modes under the following specific conditions: spray voltage, 3.0 kV; sheath gas flow rate, 40 arbitrary units; auxiliary gas, 10 arbitrary units; capillary temperature, 350 °C and vaporiser temperature, 400 °C. Nitrogen (>99.98 %) was employed as sheath, auxiliary and sweep gas. Data-dependent MS/MS acquisition was performed, where the mass spectrometer acquired full-scan data within mass-to-charge (m/z) range of 100 to 1000 m/z at a mass resolution of 80,000 and at 17,500 in case of MS/MS experiments. The five most intense ions detected in full-scan spectrum were selected for data-dependent scan with dynamic exclusion enabled. The intensity threshold for triggering the MS/MS events was set to 80,000 counts in the full-scan event. Parent ions were fragmented by high-energy C-trap dissociation (HCD) with normalised collision energy of 35 % and an activation time of 100 ms. The data-dependent acquisition permitted obtaining MS/MS data for all investigated compounds in a single run. Xcalibur[TM] software (Thermo Fisher Scientific) was employed for instrumental control and data processing. An external calibration for mass accuracy was carried out the day before the analysis according to the manufacturer's guidelines. The positive ion mode calibration solution consisted of caffeine, MRFA, Ultramark 1621 and n-butylamine in an acetonitrile/methanol/water solution containing 1 % acetic acid. The negative ion mode calibration solution consisted of sodium dodecyl sulfate, sodium taurocholate

and Ultramark 1621 in an acetonitrile/methanol/water solution containing 1 % acetic acid.

Post-acquisition data processing

MZmine v. 2.18.3 (Pluskal et al. 2010) software was used for automated detection of TPs. This software performs differential analysis of selected sets of samples by peak picking, deconvolution and alignment algorithms, comparing simultaneously thousands of MS spectra to find differentially expressed features. So, the number of compounds that need to be identified is greatly reduced, discarding spectral features also present in the control sample set and significantly increasing the throughput of complex experiments. Accurate m/z of the detected peaks was then extracted in Xcalibur[TM] (Thermo Scientific) to confirm their presence. Identification of the potential TPs was based on their accurate masses and observed isotopic patterns, obtained in the MS mode, as well as on the accurate masses of the product ions obtained in MS/MS mode.

Results and discussion

Target and non-target analysis

The performance of the UHPLC-Q Exactive hybrid quadrupole-Orbitrap MS system for ETP determination was assessed with reference standards in HPLC water (Negreira et al. 2015a). Highly selective MS chromatograms were extracted using a mass window of 5 ppm around the [M+H]$^+$ protonated molecule of ETP at 589.19212. Quantification, based on peak areas, was performed by the isotope dilution method, using ETP-d3. The measured [M+H]$^+$ were 589.1898 (−3.055 ppm) and 592.2082 (−3.711 ppm) for ETP and ETP-d3, respectively. The system provided linear responses in the range between 1 and 1000 ng/mL, with a determination coefficient (R^2) of 0.9998. Instrumental LOQ (S/N = 10) and LOD (S/N = 3) were 1.0 and 0.3 ng/mL, respectively. The repeatability in the response of the system was evaluated at two different concentrations, 50 and 500 ng/mL, for five injections performed on the same day. Relative standard deviations (RSDs, %) ranged from 0.5 to 1.3 %.

ETP has a complex structure with the basic, multi-ringed structure of the parent podophyllotoxin linked to a sugar moiety, a glucopyranoside. Its pKa value of 9.8 indicates that ETP is not likely to dissociate at environmental pH (Kosjek and Heath 2011). ETP ionised sufficiently in both positive and negative ESI mode. Based on different chromatographic conditions (see LC-MS analysis section), the compound eluted at 5.59 min. The decay of the parent compound during its biotransformation gave rise to TPs, as it is evident from their extracted ion chromatograms (see Fig. S1). However, none of these TPs could be observed as a newly formed

chromatographic peak directly from the total ion chromatograms of the biotransformation samples. One obvious reason is the high content of wastewater matrix compounds, while on the contrary, TPs usually appear in much lower concentrations. Furthermore, along with the target analyte, matrix is also biodegraded, which yields an extremely complex mixture of newly formed compounds. Of these, only a few originate from the compound of our interest, and this makes them challenging to be revealed in a complex cocktail of matrix constituents.

Data processing was performed following a metabolomics-like workflow using the software package MZmine v. 2.18.3 (Pluskal et al. 2010). Briefly, a list of ions for each scan was generated using the mass detection module (exact mass detector algorithm) followed by a chromatogram builder step. A chromatogram for each mass was constructed that could be detected continuously over the scans. Each chromatogram was then deconvoluted into individual peaks (local minimum search algorithm). After deisotoping and filtering functions, RANSAC algorithm was applied to align detected peaks in the different samples, generating an aligned peak list (including m/z, t_R and peak area) for control and treated samples (Negreira et al. 2015b). The workflow is illustrated in Fig. 2.

To visualise the data, MZmine includes several visualisation modules allowing a quick orientation of the data processed. For instance, the scatter plot (Fig. 3) has been useful for efficient comparison of the samples, showing how much one variable is affected by another. The straight line connecting the origin of scatter plot with high x and y values means that the two variables (control sample and sample after 70 h of biodegradation) are highly correlated with many ions present in both samples. The ions placed on the left side above the significant level are on average more abundant for the sample 2C1 (control sample), whereas ions located on the right side are more abundant in the sample 2C4 (after 70 h of biodegradation), and therefore, the last ions were considered as potential TPs of ETP. This kind of plots allows a rapid identification of ions showing a significant intensity change from one group to another, whereas quantitative results were observed in the form of peak lists using a table visualiser. Finally, the accurate m/z of the detected peaks was then extracted in Xcalibur to confirm their presence.

Degradation of ETP and formation of TPs

Figure 4 left shows the degradation profiles of the parent compound ETP under different experimental conditions. ETP is in the control batch (ETP-E2), i.e. in pure deionised water with no presence of minerals, nutrients or FDH and in absence of light, degraded for about 40 % in 7 days (Fig. 4 left). This degradation is less likely the consequence of biodegradation, even though it is possible, as the medium was not sterile; however, more likely, ETP was subjected to slow hydrolysis in water. The stability of ETP in ultrapure water at different temperatures had been studied before by Negreira et al. (2013), who found that ETP was fairly stable during 3 months at 4 °C and at least 24 h at 25 °C. However, the authors
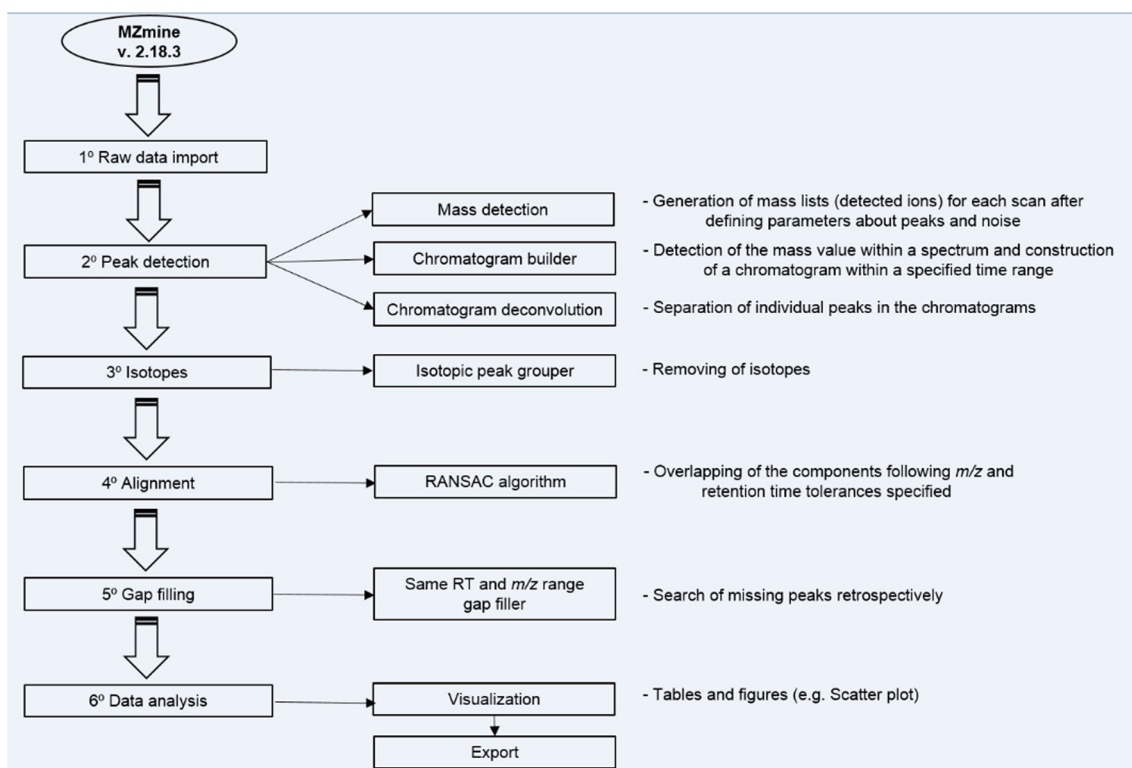

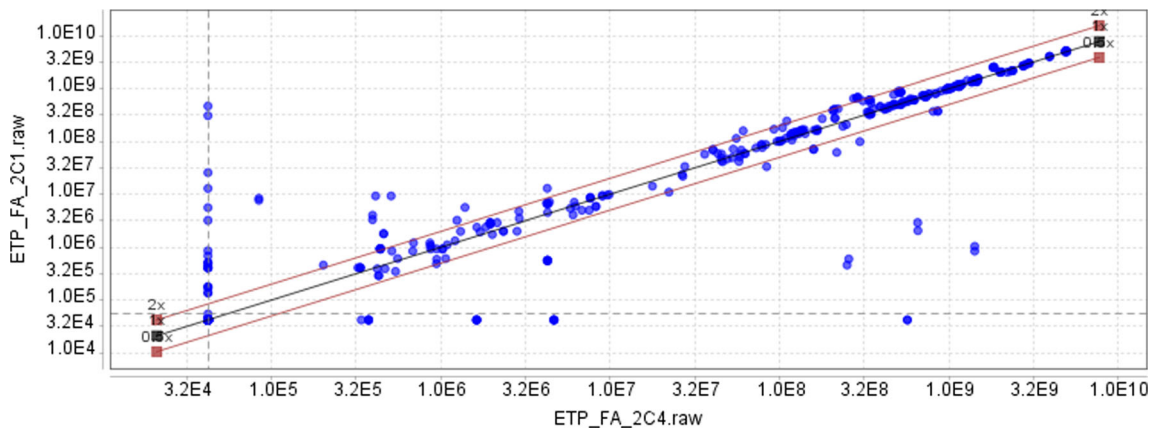**Fig. 2** Workflow of TP detection and identification

Fig. 3 Scatter plot of peak areas across the samples 2C1 (control sample) and 2C4 (after 70 h of biodegradation)

(Negreira et al. 2013) did not consider longer times than 1 day for the study of its stability at room temperature (conditions of the present work), and therefore, no direct comparison of the results is possible. It is further evident in Fig. 4 left that in batches containing nutrients at both AS concentrations, the degradation of ETP is faster than in presence of salts-only medium. On the other hand, the results of ETP degradation in the control samples, i.e. in the absence of AS or in contact with FDH-inhibited AS are inconclusive (Fig. S2). Here, the control batch (ETP-E2) and the batch with low AS concentration—abiotic in mineral medium (ETP-D2)—show very similar degradation profiles, whereas in the batch with low AS concentration—abiotic in nutrient-mineral medium (ETP-B2)—essentially no ETP degradation of any kind nor sorption to AS or glassware was observed within 7 days.

Degradation of ETP gave rise to formation of TPs. An example is TP-423, as shown in Fig. 4 right. TP-423 was found in highest amounts in the control batch (ETP-E2) and the batch with low AS concentration—abiotic in mineral medium (ETP-D2)—and in smaller quantities in the

batches with low AS concentration disregarding of the nutrient presence (ETP-A2 and ETP-C2). As evident in Fig. 4 right, the TP-423 trendline limits towards zero particularly in batch with low AS concentration in nutrient-mineral medium (ETP-A2) after 7 days of experiment, which suggests that this TP is further biodegraded by AS. This is supported by the fact that TP-423 appears in highest concentrations in the absence of microorganisms (control batch ETP-E2 and low AS concentration—abiotic in mineral medium ETP-D2), where it is not further biodegraded with both trendlines after 7 days still rising. Further, as mentioned earlier, we did not observe any degradation of ETP in the batch with low AS concentration—abiotic in nutrient-mineral medium ETP-B2 (Fig. S2), and consequently, TPs did not form. In the remaining two batches with higher concentration of AS (ETP-A and ETP-C), we observed TP-423 only in few samples, so they were not included in Fig. 4 right. In agreement with the results of the above experiments, the absence of TP-423 in the samples with high AS concentration is justified by its fast biodegradation.
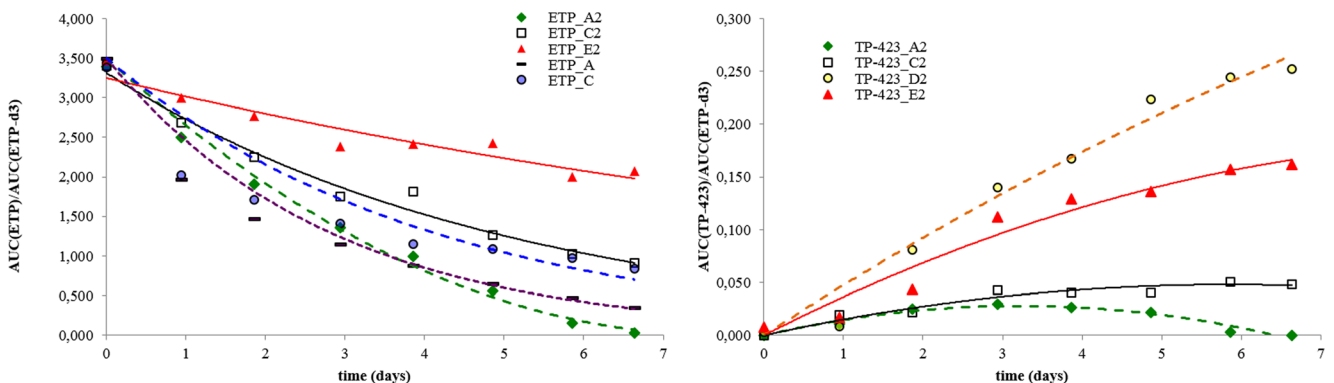

Fig. 4 *Left*: Biodegradation profiles of ETP at two different AS concentrations (batches A2 and C2 vs. A and C) and in the presence/absence of nutrient medium (batches A and A2 vs. C and C2). E2: control batch (for details, refer to Table 1). *Right*: Formation of TP-423 in different batches. AUC: peak area

TP-629 (Fig. S3) shows very similar formation profiles to those of TP-423, despite that in this case, the TP was also observed in batches with high AS concentration (ETP-A and ETP-C).

TP-643 was not found in batches containing FDH-inhibited AS nor in batches with high concentration of AS (A and C), whereas in the control batch E2, it was found in trace levels (Fig. S4). As there are substantial amounts of TP-643 in the batches with low AS concentration (ETP-A2 and ETP-C2) that are after day 7 still increasing, we propose that TP-643 is a product of biodegradation, which is fairly resistant to further biodegradation. In regards to its chemical structure, which is discussed under the next section (see Identification of TPs section and Fig. S9), we suppose that the compound is formed from TP-629, which is in agreement with the degradation profile of the latter (Fig. S3), where the trendline turns back towards zero after day 4, particularly in batches with low AS concentration (ETP-C2 and ETP-A2).

TP-609 (Fig. S5) was found in all batches disregarding the AS concentration, but it appeared later in the course of the biodegradation experiment, i.e. in the batch with low AS concentration in nutrient-mineral medium (ETP-A2), the compound was found only in the samples from day 3 to day 7. It was found present in highest amounts in the control batch (ETP-E2) and in lowest quantities in the batch with low AS concentration under abiotic conditions in the presence of minerals only (ETP-D2), whereas it did not appear in the batch with low AS concentration under abiotic conditions in the presence of nutrient-mineral medium (ETP-B2). Based on these results, we suggest that the compound can be formed though either an abiotic breakdown or by biodegradation.

Picro-ETP (Fig. S6) is a transient species formed within the first 24 h after the start of the experiment, but on day 4, its degradation rate exceeds its formation. The exemption are batches with high AS content (ETP-A and ETP-C), where the compound appears later in the course of the experiment. Similar to other identified TPs, it is evident that its formation is either abiotic or microbiological.

Identification of TPs

Table 2 shows the chromatographic and MS data of ETP and its TPs. The fragmentation patterns of ETP and its TPs are very complex giving a number of fragment ions that correspond to molecular formulae from which several different structural isomers can be derived for each species. For this reason, we herein propose those structures we believe are most stable and most illustrative for particular species.

The MS spectrum of ETP (Fig. 5) shows the sodium adduct at $[M+Na]^+$ 611.17 with the molecular formula $C_{29}H_{32}O_{13}Na^+$. Two most abundant fragment ions are seen at m/z 229.05 and m/z 185.06, which stand for the central tetracyclic and the tricyclic ring systems after the loss of dioxolane ring (ring A), respectively. The structures of the fragment ions have before not been resolved into detail, but the characteristic fragments including m/z 185.06, m/z 229.05, m/z 299.09 and m/z 383.11 are in agreement with Vairamani et al. (1996), Chen and Uckun (2000) and Zhao et al. (2008). Another important fragment ion is at m/z 383.11, which demonstrates a loss of the glycoside. Other fragment ions merely exhibit the losses of methoxy or hydroxyl groups or cleavage of ethylidene-glucopyranoside ring and fractionation of water molecule (Fig. 5).

TP-629 shows the $[M+Na]^+$ mass at 629.18 with the molecular formula $C_{29}H_{34}O_{14}Na^+$ suggesting an additional oxygen and two hydrogens attached to the ETP molecule. Despite this minor structural alteration with regards to ETP, the mass spectrum (Fig. 6, top) of TP-629 shows fundamental differences including two most distinctive fragment ions at m/z 393.09 and m/z 229.07. Provided by the high resolving power of the Orbitrap MS, the careful inspection of the latter fragment ion shows also the m/z 229.05 corresponding to the characteristic $C_{13}H_9O_4^+$ (see also Fig. 5) as evident in Fig. 6 (bottom). Other fragment ions that characterise this TP and are not involved in the ETP mass spectrum are found at m/z 349.10 and m/z 120.08. The fragment ions at m/z 393.09, m/z 349.10 and m/z 229.07 all suggest that the glucopyranoside-derived structure remains involved in the TP-629, which gives an indication on its stability and implies that the biotransformation most likely occurred in this part of the molecule. For this reason and because of the existence of 3-(1-hydroxyethoxy)propan-1-ol at m/z 120.08, we propose that TP-629 is formed by a cleavage of the ethylidene-glucopyranoside C–O bond and addition of a water molecule.

TP-423 with the protonated molecule found at $[M+H]^+$ 401.12 and a molecular formula of $C_{21}H_{21}O_8^+$ also shows the sodium adduct at $[M+Na]^+$ 423.10. TP-423 was found at t_R 5.41 min and was first subjected to the loss of water yielding its most abundant ion at m/z 383.11. The latter is common to ETP and reveals the MSMS spectrum shown in Fig. S7. Generally, TP-423 and ETP exhibit similar mass spectra excluding the fragment ions higher than m/z 383.11 (see Fig. 5 and Fig. S7). However, the relative abundances of their fragment ions do differ, which may be the consequence of the collision energy applied to different parent ions. Based on the fragmentation pattern, we conclude that the TP-423 is formed by the loss of glycoside from the parent molecule and is assigned to ETP-aglycone, named also 4′-demethylepipodophyllotoxin.

Table 2 Accurate mass measurements of ETP and its TPs as determined by LC-Q-Orbitrap MS in MS or MS/MS mode

Compound	Nominal ion mass	Chromatographic retention time	Measured mass (m/z)	Mass error (mmu)	Molecular formula	RDB
ETP	589 $[M+H]^+$	5.59 min	589.18976	−2.356	$C_{29}H_{33}O_{13}^+$	13.5
	611 $[M+Na]^+$		611.17165	−2.410	$C_{29}H_{32}O_{13}Na^+$	13.5
	405		405.09305	−3.829	$C_{23}H_{17}O_7^+$	15.5
	383		383.11099	−2.088	$C_{21}H_{19}O_7^+$	12.5
	305		305.07944	−1.395	$C_{19}H_{13}O_4^+$	13.5
	299		299.08994	−1.460	$C_{17}H_{15}O_5^+$	10.5
	267		267.06448	−0.705	$C_{16}H_{11}O_4^+$	11.5
	247		247.05753	−2.570	$C_{13}H_{11}O_5^+$	8.5
	239		239.06956	−0.711	$C_{15}H_{11}O_3^+$	10.5
	229		229.04852	−1.015	$C_{13}H_9O_4^+$	9.5
	199		199.03841	−0.561	$C_{12}H_7O_3^+$	9.5
	185		185.05894	−0.766	$C_{12}H_9O_2^+$	8.5
	173		173.05931	−0.396	$C_{11}H_9O_2^+$	7.5
	123		123.04156	−2.496	$C_7H_7O_2^+$	4.5
	85		85.02863	0.224	$C_4H_5O_2^+$	2.5
Picro-ETP	405	5.74 min	405.09305	−3.829	$C_{23}H_{17}O_7^+$	15.5
	365		365.10117	−0.759	$C_{21}H_{17}O_6^+$	13.5
	324		324.09787	−1.355	$C_{19}H_{16}O_5$	12.0
	299		299.09079	−0.610	$C_{17}H_{15}O_5^+$	10.5
	267		267.06427	−0.915	$C_{16}H_{11}O_4^+$	11.5
	239		239.06932	−0.951	$C_{15}H_{11}O_3^+$	10.5
	229		229.04866	−0.875	$C_{13}H_9O_4^+$	9.5
	185		185.05893	−0.776	$C_{12}H_9O_2^+$	8.5
	167		167.06981	−0.461	$C_9H_{11}O_3^+$	4.5
	107		107.04951	0.369	$C_7H_7O^+$	4.5
	85		85.02864	0.234	$C_4H_5O_2^+$	2.5
TP-629	629	5.42 min	629.18161	−2.467	$C_{29}H_{34}O_{14}Na^+$	12.5
	393		393.09280	−4.628	$C_{22}H_{17}O_7^+$	14.5
	349		349.10571	−1.889	$C_{21}H_{17}O_5^+$	13.5
	307		307.06925	−0.235	$C_{19}H_{15}O_4^+$	12.5
	299		299.08948	−2.468	$C_{17}H_{15}O_5^+$	10.5
	267		267.06445	−1.284	$C_{16}H_{11}O_4^+$	11.5
	239		239.06842	−1.851	$C_{15}H_{11}O_3^+$	10.5
	229		229.06735	−3.315	$C_{10}H_{13}O_6^+$	4.5
	229		229.04765	−1.885	$C_{13}H_9O_4^+$	9.5
	199		199.03802	−0.951	$C_{12}H_7O_3^+$	9.5
	185		185.05930	−0.406	$C_{12}H_9O_2^+$	8.5
	173		173.05963	−0.076	$C_{11}H_9O_2^+$	7.5
	120		120.08082	2.742	$C_5H_{12}O_3$	0.0
TP-643	643	5.51 min/5.62 min	643.16111	−2.231	$C_{29}H_{32}O_{15}Na^+$	13.5
	621		621.17958	−1.817	$C_{29}H_{33}O_{15}^+$	13.5
	567		567.14337	−6.333	$C_{29}H_{27}O_{12}^+$	16.5
	437		437.08371	−2.999	$C_{23}H_{17}O_9^+$	15.5
	393		393.09308	−3.799	$C_{22}H_{17}O_7^+$	14.5
	379		379.07916	−2.069	$C_{21}H_{15}O_7^+$	14.5
	367		367.07764	−3.589	$C_{20}H_{15}O_7^+$	13.5
	351		351.04794	−1.989	$C_{19}H_{11}O_7^+$	14.5
	339		339.08368	−2.635	$C_{19}H_{15}O_6^+$	12.5

Table 2 (continued)

Compound	Nominal ion mass	Chromatographic retention time	Measured mass (*m/z*)	Mass error (mmu)	Molecular formula	RDB
	325		325.07013	−0.535	$C_{18}H_{13}O_6^+$	12.5
	307		307.05878	−1.320	$C_{18}H_{11}O_5^+$	13.5
	299		299.05441	−0.605	$C_{11}H_{11}O_6^+$	11.5
	281		281.08005	−0.785	$C_{17}H_{13}O_4^+$	11.5
	263		263.06979	−0.481	$C_{17}H_{11}O_3^+$	12.5
	255		255.06422	−0.965	$C_{15}H_{11}O_4^+$	10.5
	249		249.05324	−1.381	$C_{16}H_9O_3^+$	12.5
	227		227.06949	−0.781	$C_{14}H_{11}O_3^+$	9.5
	225		223.07419	−1.166	$C_{15}H_{11}O_2^+$	10.5
	212		212.04597	−0.826	$C_{13}H_8O_3$	10.0
	199		199.07481	−0.546	$C_{13}H_{11}O_2^+$	8.5
	185		185.05943	−0.276	$C_{12}H_9O_2^+$	8.5
	161		161.05937	−0.336	$C_{10}H_9O_2^+$	6.5
	141		141.05438	−0.241	$C_7H_9O_3^+$	3.5
	107		107.01017	−2.586	$C_6H_3O_2^+$	5.5
	85		85.02882	0.414	$C_4H_5O_2^+$	2.5
	75		75.04450	0.444	$C_3H_7O_2^+$	0.5
TP-609	609	6.02 min	609.15546	−2.402	$C_{29}H_{30}O_{13}Na^+$	14.5
	587		587.17410	−2.366	$C_{29}H_{31}O_{13}^+$	14.5
	549		549.13647	−3.216	$C_{29}H_{25}O_{11}^+$	17.5
	421		421.08801	−3.784	$C_{23}H_{17}O_8^+$	15.5
	403		403.07730	−3.929	$C_{23}H_{15}O_7^+$	16.5
	381		381.09512	−1.759	$C_{21}H_{17}O_7^+$	13.5
	349		349.06931	−1.355	$C_{20}H_{13}O_6^+$	14.5
	337		337.10565	−1.400	$C_{20}H_{17}O_5^+$	12.5
	319		319.05722	−2.880	$C_{19}H_{11}O_5^+$	14.5
	305		305.07858	−2.255	$C_{19}H_{13}O_4^+$	13.5
	291		291.06427	−0.915	$C_{18}H_{11}O_4^+$	13.5
	277		277.08408	−1.841	$C_{18}H_{13}O_3^+$	12.5
	247		247.07475	−0.606	$C_{17}H_{11}O_2^+$	12.5
	219		219.07875	−1.692	$C_{16}H_{11}O^+$	11.5
TP-423	423	5.41	423.10298	−2.059	$C_{21}H_{20}O_8Na^+$	11.5
	401		401.12139	−1.704	$C_{21}H_{21}O_8^+$	11.5
	383		383.11246	−0.069	$C_{21}H_{19}O_7^+$	12.5
	365		365.10129	−0.675	$C_{21}H_{17}O_6^+$	13.5
	305		305.07944	−1.395	$C_{19}H_{13}O_4^+$	13.5
	277		277.08456	−1.361	$C_{18}H_{13}O_3^+$	12.5
	267		267.06412	−1.065	$C_{16}H_{11}O_4^+$	11.5
	247		247.07428	−1.076	$C_{17}H_{11}O_2^+$	12.5
	229		229.04866	−0.875	$C_{13}H_9O_4^+$	9.5
	185		185.05914	−0.566	$C_{12}H_9O_2^+$	8.5
	167		167.06989	−0.381	$C_9H_{11}O_3^+$	4.5
	135		135.04369	−0.366	$C_8H_7O_2^+$	5.5
	85		85.02879	−0.384	$C_4H_5O_2^+$	2.5

RDB ring double bond equivalent

Figure S8 shows ESI(+) MSMS spectrum of TP-609, which appears as the sodium adduct with the molecular formula $C_{29}H_{30}O_{13}Na^+$, that is two hydrogens less than the parent ETP giving an implication on additional unsaturated
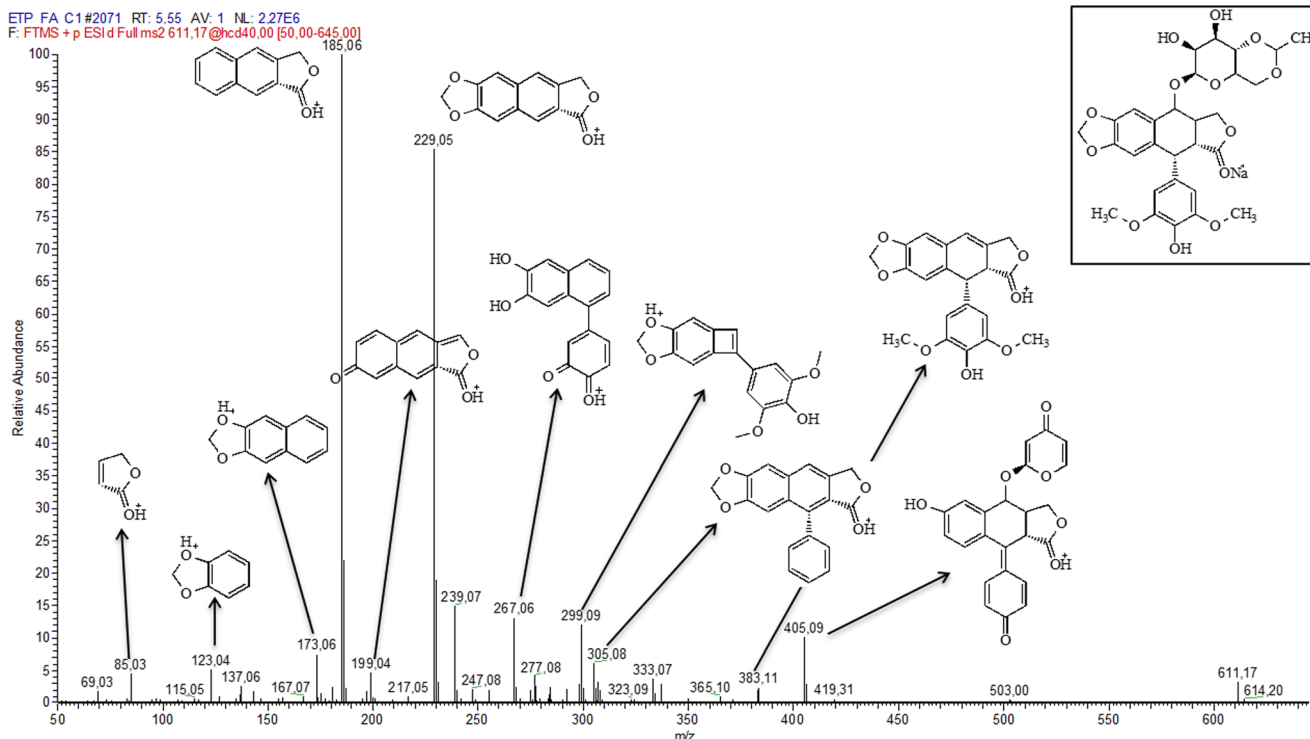
Fig. 5 ESI(+) MSMS spectrum of ETP

bond in the TP-609 molecule. In the mass spectrum of TP-609, we propose several fragment ions (m/z 219.08, m/z 247.07, m/z 277.08, m/z 305, m/z 319.06, m/z 349.07, m/z 403.08, m/z 421.09, m/z 549.14) involving a stable aromatic naphthalene system (rings B + C) instead of an unsaturated one. The latter commonly appears in ETP fragment ions and other in TPs' mass spectra. The aromaticity is in most fragment ions achieved by cleavage of the glycoside bond or by loss of a water molecule and subsequent delocalisation of the double bond to the dihydronaphthalene ring system (B + C). For this reason, we propose that TP-609 is formed by dehydrogenation of ETP tetrahydronaphthalene ring.

In comparison to the parent compound, the molecular formula of TP-643 ([M+Na]$^+$ 643.16 corresponding to $C_{29}H_{32}O_{15}Na^+$) shows two additional oxygen atoms in its molecular structure. Its mass spectrum (Fig. S9) shows several fragment ions common to ETP including m/z 85.03, m/z 185.06 and m/z 199.07. In particular, the latter two are important and demonstrate that rings B, C and D, i.e. tetrahydronaphthalene (B + C), with attached γ-lactone ring (D), remained intact. However, m/z 229.05, m/z 305.08 and m/z 383.11 (Fig. 5) are missing in the TP-643 MSMS spectrum indicating that dioxolane ring was altered during the biotransformation. Several fragment ions in the TP-643 MSMS spectrum however imply that the dioxolane ring was oxidised into dioxolane-2-one. Glycoside bond was again among the first to cleave in the TP-643 structure, so there are not many fragment ions to support this. Yet,

taking into account the structure of the m/z 567.14, we believe that the same type of ethylidene cleavage and water addition occurred as in case of TP-629.

Approximately 0.15 min after ETP, a compound with the same protonated molecule, sodium adduct and the same molecular formula as ETP eluted. In its MSMS spectrum (Fig. S10), the same fragment ions are evident, though their abundances differ from those in ETP MSMS spectrum. In our opinion, this compound is most likely picroetoposide, which was before mentioned by Liliemark et al. (1995), Beijnen et al. (1988), Zhao et al. (2008) and Dow et al. (1983). As reported, the *trans*-fused γ-lactone D ring in podophyllotoxin and its analogues are susceptible to isomerisation to picropodophyllin with the *cis*-fused γ-lactone D ring, when exposed to a mild base (Zhao et al. 2008; Beijnen et al. 1988). The pH of wastewater mixture applied in our experiment was at approximately 8, which provides appropriate conditions for ETP to undergo isomerisation. Isomerisation to inactive *cis*-lactone also occurs in plasma (Liliemark et al. 1995). The stereochemistry of the *trans*-lactone is essential for cytotoxicity of etoposide, where *cis*-lactone was found biologically inactive (Dow et al. 1983; Liliemark et al. 1995).

Finally, at the retention time of 5.22 min, there was also a peak with [M+Na]$^+$ 229.07 corresponding to $C_8H_{14}O_6Na^+$, the glycoside component of the ETP molecule. We were unable to confirm its structure with MSMS, because of its insufficient abundance.
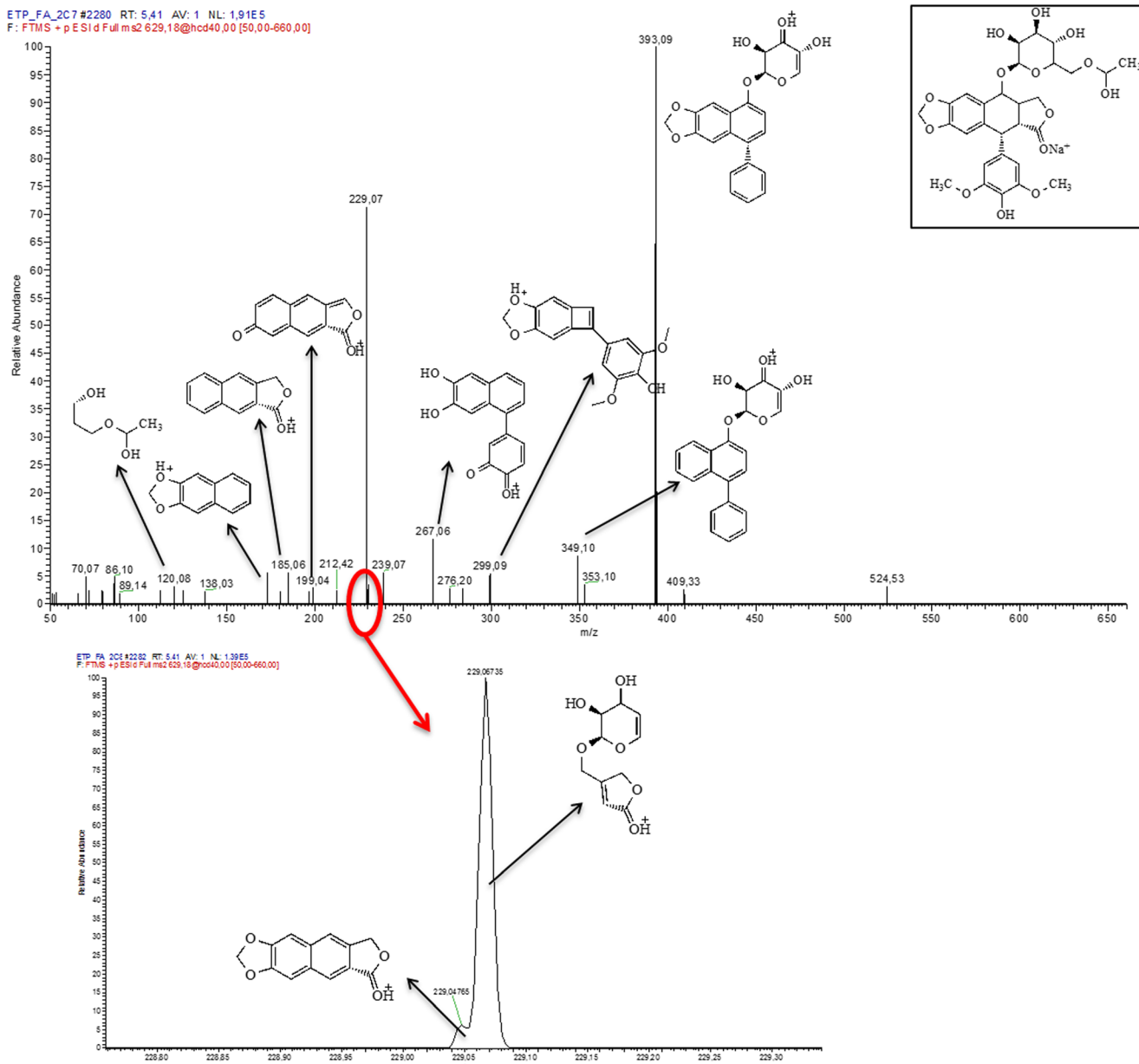
Fig. 6 *Top*: ESI(+) MSMS spectrum of TP-629 with proposed chemical structures of fragment ions; *bottom*: zoomed fragment ion at *m/z* 229 with the corresponding two chemical structures

Conclusions

This study reports on the biodegradation of ETP, a cytostatic compound so far rarely addressed in the literature. It was observed that in the artificial wastewater containing nutrients and salts and in the presence of activated sludge up to 99.9 %, ETP was degraded in 7 days, where about 40 % was abiotic and the remaining fraction was assigned to biodegradation. We showed that the biodegradation of ETP and formation of its TPs highly depend on the composition of wastewater, e.g. the presence of nutrients and minerals and concentration of activated sludge. Q Exactive hybrid quadrupole-Orbitrap tandem MS was used for analysis, enabling concurrent structural

elucidation of the TPs and quantitative analysis in a single run. Five TPs were proposed, among them a product of glycoside bond hydrolysis, dehydrogenation, oxidation of dioxolane ring, ring cleavage with hydroxylation in the glycoside segment, whereas one TP was a product of the latter two listed reactions. Based on degradation profiles and kinetics, some TPs were suggested to be a result of biodegradation, whereas others were more likely originating from abiotic reactions. An illustrative example is TP-423, which is most likely a product of hydrolysis, but due to high AS concentration, this TP was further biodegraded as soon as it was formed.

Given the fact that a majority of the identified TPs were products of minor alterations in the ETP molecule, there are

probably many more TPs, some of them insufficiently stabile, others not abundant enough, inadequately ionised by electrospray or chromatographically not favoured to be detected and identified by the applied analytical method. Further investigations in this field are necessary including studies on occurrence and effects of the identified compounds in sewerage works and in the environment. Finally, based on the ETP classification amongst most carcinogen substances and taking into account the very minor structural alterations of the TPs identified herein, these compounds potentially exhibit similar adverse effects on non-target organisms, so their potency should be assessed and necessary precautions taken to limit their entrance into the environment.

References

Akhtar N, Talegaonkar S, Kishan Khar R, Jaggi M (2013) A validated stability-indicating LC method for estimation of etoposide in bulk and optimized self-nano emulsifying formulation: kinetics and stability effects. Saudi Pharm J 21:103–111

Beijnen JH, Holthuis JJM, Kerkdijk HG, van der Houwen OAGJ, Paalman ACA, Bult A, Underberg WJM (1988) Degradation kinetics of etoposide in aqueous solution. Int J Pharm 41:169–178

Chen C-L, Uckun FM (2000) Highly sensitive liquid chromatography-electrospray mass spectrometry (LC-MS) method for the determination of etoposide levels in human serum and plasma. J Chromatogr B 744:91–98

Donner E, Kosjek T, Qualmann S, Kusk KO, Heath E, Revitt DM, Ledin A, Andersen HR (2013) Ecotoxicity of carbamazepine and its UV photolysis transformation products. Sci Total Environ 443:870–876

Dow LW, Sinkule JA, Look T, Horvath A, Evans WE (1983) Comparative cytotoxic and cytokinetic effects of the epipodophyllotoxins 4′-demethylepipodophyllotoxin-9-(4,6-O-2-ethylidene-β-d-glucopyranoside) and 4′-demethylepipodophyllotoxin-9-(4,6-O-2-thenylidene-β-d-glucopyranoside) and their metabolites on human. Cancer Res 43:5699–5706

Ferrando-Climent L, Rodriguez-Mozaz S, Barceló D (2013) Development of a UPLC-MS/MS method for the determination of ten anticancer drugs in hospital and urban wastewaters, and its application for the screening of human metabolites assisted by information-dependent acquisition tool (IDA) in sewage samples. Anal Bioanal Chem 405:5937–52

Ferrando-Climent L, Rodriguez-Mozaz S, Barceló D (2014) Incidence of anticancer drugs in an aquatic urban system: from hospital effluents through urban wastewater to natural environment. Environ Pollut 193:216–223

Franquet-Griell H, Gómez-Canela C, Ventura F, Lacorte S (2015) Predicting concentrations of cytostatic drugs in sewage effluents and surface waters of Catalonia (NE Spain). Environ Res 138:161–172

Haim N, Nemec J, Roman J, Sinha BK (1987) In vitro metabolism of etoposide (VP-16-213) by liver microsomes and irreversible binding of reactive intermediates to microsomal proteins. Biochem Pharmacol 36:527–536

Hande KR (2008) Topoisomerase II inhibitors. Update Cancer Ther 3: 13–26

Holthuis JJ, Postmus PE, Van Oort WJ, Hulshoff B, Verleun H, Sleijfer DT et al (1986) Pharmacokinetics of high dose etoposide (VP 16–213). Eur J Cancer Clin Oncol 22:1149–55

International Agency for Research on Cancer (IARC) (2012) http://monographs.iarc.fr/ENG/Classification/latest_classif.php/Volumes 1–114 (accessed 10th February 2016).

Kosjek T, Heath E, Kompare B (2007) Anal Bioanal Chem 387:1379–87

Kosjek T, Heath E (2011) Occurrence, fate and determination of cytostatic pharmaceuticals in the environment. TrAC, Trends Anal Chem 30:1065–87

Kosjek T, Perko S, Žigon D, Heath E (2013) Fluorouracil in the environment: analysis, occurrence, degradation and transformation. J Chromatogr A 1290:62–72

Liliemark E, Pettersson B, Peterson C, Liliemark J (1995) High-performance liquid chromatography with fluorimetric detection for monitoring of etoposide and its cis-isomer in plasma and leukaemic cells. J Chromatogr B: Biomedical Sciences and Applications 669:311–317

Martin J, Camacho-Munoz D, Santos JL, Aparicio I, Alonso E (2011) Simultaneous determination of a selected group of cytostatic drugs in water using high-performance liquid chromatography-triple-quadrupole mass spectrometry. J Sep Sci 34:3166–77

Negreira N, López de Alda M, Barceló D (2015a) Degradation of the cytostatic etoposide in chlorinated water by liquid chromatography coupled to quadrupole-Orbitrap mass spectrometry: identification and quantification of by-products in real water samples. Sci Total Environ 506–507:36–45

Negreira N, Mastroianni N, López de Alda M, Barceló D (2013) Multianalyte determination of 24 cytostatics and metabolites by liquid chromatography–electrospray–tandem mass spectrometry and study of their stability and optimum storage conditions in aqueous solution. Talanta 116:290–299

Negreira N, Regueiro J, Lopez de Alda M, Barcelo D (2015b) Degradation of the anticancer drug erlotinib during water chlorination: non-targeted approach for the identification of transformation products. Water Res 85:103–113

Pluskal T, Castillo S, Villar-Briones A, Orešič M (2010) MZmine 2: modular framework for processing, visualizing, and analyzing mass spectrometry-based molecular profile data. BMC Bioinformatics 11:395

Süzer Ö. University of Istanbul. http://www.ctf.edu.tr/farma/onersuzer/pdf/ing/05_Dysinfectant.pdf (accessed 25th December 2013).

Vairamani M, Suma K, Kamal A, Gayatari NL (1996) Mass spectral study of etoposide. Rapid Commun Mass Sp 10:817–820

Yin J, Shao B, Zhang J, Li (2010) A preliminary study on the occurrence of cytostatic drugs in hospital effluents in Beijing, China. Bull Environ Contam Toxicol 84:39–45

Zhao L, Tian X, Fan P-C, Zhan Y-J, Shen D-W, Jin Y (2008) Separation, determination and identification of the diastereoisomers of podophyllotoxin and its esters by high-performance liquid chromatography/tandem mass spectrometry. J Chromatogr A 1210:168–177

Zounková R, Odráška P, Doležalová L, Hilscherová K, Maršálek B, Bláha L (2007) Ecotoxicity and genotoxicity assessment of cytostatic pharmaceuticals. Environ Toxicol Chem 26:2208–2214